COMPARISON OF CASIMIR, ELASTIC, ELECTROSTATIC FORCES FOR A MICRO-CANTILEVER

by

AMMAR ALHASAN
B.S. AL-Mustansiry University, 2008

A thesis submitted in partial fulfillment of the requirements
for the degree of Masters of Science
in the Department of Physics
in the College of Science
at the University of Central Florida
Orlando, Florida

Spring Term
2014

Major Professor: Robert E. Peale

ABSTRACT

Casimir force is a cause of stiction (adhesion) between metal surfaces in Micro-Electro Mechanical Systems (MEMS). Casimir Force depends strongly on the separation of the two surfaces and the contact area. This thesis reviews the theory and prior experimental demonstrations of the Casimir force. Then the Casimir attractive force is calculated for a particular MEMS cantilever device, in which the metal cantilever tip is required to repeatedly touch and release from a metal tip pad on the substrate surface in response to a periodic driving electrostatic force. The elastic force due to the bending of the cantilever support arms is also a consideration in the device operation. The three forces are calculated analytically and compared as a function of cantilever tip height. Calculation of the electrostatic force uses coefficients of capacitance and electrostatic induction determined numerically by the finite element method, including the effect of permittivity for the structural oxide. A condition on the tip area to allow electrostatic release of the tip from the surface against Casimir sticking and elastic restoring forces is established.

Dedicated to:

HCED Iraq and my parents

ACKNOWLEDMENTS

Words cannot describe the gratitude that I have for my advisor Dr. Robert Peale. Without his help and guidance, this thesis could never have been accomplished. He has assisted in every aspect of my research and I am truly grateful for allowing me to work in his research group,

I would also like to warmly thank Dr. Enrique Del_Barco_ and Dr. Lee Chow for serving on my thesis committee and taking the time reading and evaluating my thesis and providing me with invaluable insight.

I would also like to acknowledge Imen Rezadad for his role in assisting me in various technical aspects of my research especially to learn how to work on the simulation by using Elmer program. Also, thanks to Evan Smith and Javaneh Boroumand for their assistance on introducing me to the proper techniques to work with and maintain equipment related to my research. Working with them, and learning from their experience has been extremely beneficial for me. I would also thank Mehmet Yesiltas for his helping in digitizing the data. Throughout my research I have been blessed enough to receive great suggestions and comments from my group members and my friends and I want to thank all of them. Also I would thank my parents who have been supporting me. I wish to acknowledge my government and the program HCED for supporting me during all these years and giving me the opportunity to advance my academic career in the United States. Above all, I give thanks to God for all the good things that I have learned.

TABLE OF CONTENTS

LIST OF FIGURES

INTRODUCTION

Quantum electrodynamics (QED) predicts a force between two closely spaced objects due to quantum electromagnetic fluctuations. For metals, the force was first studied by Casimir (1948) and is hence known as the Casimir force. Two perfectly conducting, uncharged, closely spaced, parallel flat plates in vacuum attract due to exclusion of electromagnetic modes between them. This is a purely quantum-mechanical effect arising from the zero-point energy of the harmonic oscillators that are the normal modes of the electromagnetic field [1]. The Casimir force depends on geometry [2]. Casimir force becomes large at small separations, equaling ~1 atmosphere of pressure at 10 nm separation [3].

Fig. 1 explains qualitatively the origin of the Casimir force. The number of different frequencies per unit frequency interval is $V\,\omega^2/2\pi^2c^3$ [4], i.e. it is proportional to volume. As the volume between to metal places decreases, fewer modes are supported in comparison to the number of modes outside the plates. Thus, the radiation on the inner surfaces of the conduction plates is less. Fig. 1 suggests this schematically by showing that the space between the plates supports only short wavelength modes, while the space outside supports additional long-wavelength ones.

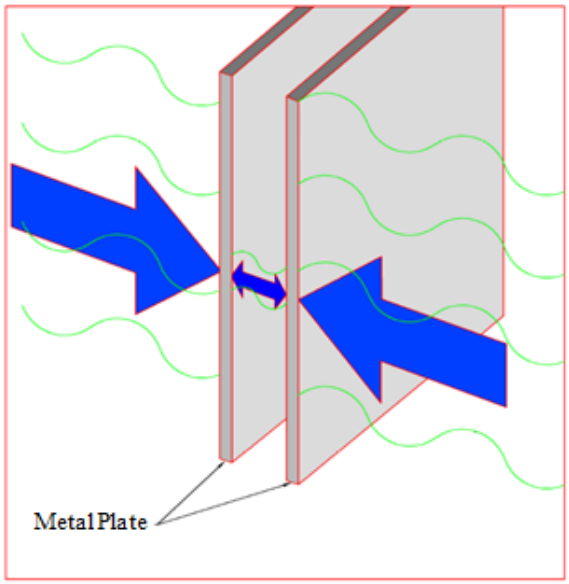

Figure 1: Two metal plates are closely spaced. The number of modes outside the plates is large because the volume is large. The number of modes in the space between the plates is smaller because fewer modes can satisfy the boundary conditions. Thus the radiation pressure on the outer plate surfaces exceeds that on the inner surfaces, resulting in an attraction.

Casimir and van der Waals forces are quite different. The van der Waals force is due to dipole-dipole interactions between molecules and is always attractive [2]. However, the physics responsible for the Casimir force can give rise to either attraction or repulsion, depending on the permittivity of the materials involved. Thus, the attractive Casimir force for metal surfaces in vacuum is a special case of the more general Casimir-Lifshitz force [5]. This thesis considers only the attractive Casimir forces between metal plates in vacuum.

Casimir force is usually very weak compared with electric forces except at very small distances. It may be strong compared to gravitational force as in MEMS where the latter force scales as volume and is completely negligible. The importance of surface effects (e.g. Casimir force) to volume effects (gravitational force) grows as 1/L with decreasing length scale L.

CHAPTER ONE: THEORETICAL CONSIDERATIONS

We consider the zero point electromagnetic energy in a box, which is assumed to be a rectangular parallelepiped with perfectly conducting walls of area L x L and separation d. Electromagnetic waves inside the box must have nodes on the walls, which restricts and discretizes the possible frequencies. This causes a dependence on the wall separation d of the zero point energy, which results in a force on the walls. Smaller volume between the walls causes smaller the zero point energy, so that energy is lowered when the walls move closer. Thus, the force is attractive

The boundary conditions require that integral numbers of half wavelengths exist between each pair of walls. For example, the wavelength of an electromagnetic wave traveling (e.g.) in the short direction of the box must satisfy $n\lambda/2 = d$, giving a wave vector $k_z = n\pi/d$, where n is an integer. Taking into account all possible propagation directions, the allowed frequencies are

$$\omega_{lmn} = \pi c\left(\frac{l^2}{L^2} + \frac{m^2}{L^2} + \frac{n^2}{d^2}\right)^{\frac{1}{2}} \qquad (1.1)$$

where each mode is enumerated by three positive integers l, m, and n. The electromagnetic field is quantized with energy

$$E = \sum_{l,m,n} 2\hbar\omega_{l,m,n}\left(N_{lmn} + \frac{1}{2}\right) \qquad (1.2)$$

Where N_{lmn} is the number of quanta in the lmn^{th} mode. The factor of 2 accounts for two-fold degeneracy of every frequency for which all the l,m,n are non-zero (Appendix A). The zero point energy corresponds to zero quanta in any mode, or

$$E_0 = \sum_{l,m,n} \hbar\omega_{l,m,n} = \sum'_{l,m,n} \hbar c\left(\frac{l^2\pi^2}{L^2} + \frac{m^2\pi^2}{L^2} + \frac{n^2\pi^2}{d^2}\right)^{\frac{1}{2}} \quad (1.3)$$

The prime indicates that when one of these integers is equal to zero there should be a factor one half because such frequencies are non-degenerate (Appendix A). When two of the integers are zero, there is no electric field at all (Appendix A).

Because L >> d, the density of modes is much larger in the transverse directions than in the longitudinal direction of the cavity, so that the sums over indices *l* and *m* may be converted to integrals over wavenumbers, using $dk_x = \frac{\pi}{L} dn$, etc.

$$E_0(d) = \frac{\hbar c L^2}{\pi^2} \sum'_n \int_0^\infty dk_x \int_0^\infty dk_y \left(k_x^2 + k_y^2 + \frac{n^2\pi^2}{d^2}\right)^{\frac{1}{2}} \quad (1.4)$$

For large plate separations, the sum over *n* is similarly replaced by an integral giving

$$E_0(\infty) = \frac{\hbar c L^2 d}{\pi^3} \iiint_0^\infty (u^2 + v^2 + w^2)^{\frac{1}{2}} du dv dw \quad (1.5)$$

The energy required to bring the plates from a large distance to a separation d is

$$U(d) = E_0(d) - E_0(\infty)$$

$$= \frac{\hbar c L^2}{\pi^2} \left[\sum'_n \iint_0^\infty \left(u^2 + v^2 + \frac{\pi^2 n^2}{d^2}\right)^{\frac{1}{2}} du dv - \frac{d}{\pi} \iiint_0^\infty (u^2 + v^2 + w^2)^{\frac{1}{2}} du dv dw \right] \quad (1.6)$$

Transforming to cylindrical polar coordinates ($u^2 + v^2 = r^2$, d*u*d*v* = r dr dθ), with the integral over θ giving π/2 since the original integral is over positive values of *u* and *v* only, gives

$$U(d) = \frac{\hbar c L^2}{2\pi} \left[\sum_{n=0}^\infty \int_0^\infty \left(r^2 + \frac{n^2\pi^2}{d^2}\right)^{\frac{1}{2}} r dr - \frac{d}{\pi} \int_0^\infty dw \int_0^\infty (r^2 + w^2)^{\frac{1}{2}} r dr\right] \quad (1.7)$$

In the second integral, substitute $w' = \frac{d}{\pi} w$, and then drop the primes to get

$$U(d) = \frac{\hbar c L^2}{2\pi} \left[\sum_{n=0}^\infty \int_0^\infty \left(r^2 + \frac{\pi^2}{d^2} n^2\right)^{\frac{1}{2}} r dr - \int_0^\infty dw \int_0^\infty \left(r^2 + \frac{\pi^2}{d^2} w^2\right)^{\frac{1}{2}} r dr\right] \quad (1.8)$$

The change of variables $x = d^2r^2/\pi^2$ gives

$$U(d) = \frac{\hbar c L^2}{4\pi}\frac{\pi^3}{d^3}\left[\sum_{n=0}^{\infty}\int_0^{\infty} dx(x+n^2)^{\frac{1}{2}} - \int_0^{\infty} dw \int_0^{\infty} dx(x+w^2)^{\frac{1}{2}}\right] \quad (1.9)$$

The function

$$F(u) \equiv \int_0^{\infty} dx(x+u^2)^{\frac{1}{2}} \quad (1.10)$$

Appears in both terms of Eq. (1.9), so that

$$U(d) = \frac{\pi^2\hbar c}{4d^3}L^2\left[\frac{1}{2}F(0) + \sum_{n=1}^{\infty}F(n) - \int_0^{\infty} dwF(w)\right] \quad (1.11)$$

We evaluate this difference using the Euler-Maclaurin Formula (see Appendix B)

$$\sum_{n=1}^{\infty}F(n) - \int_0^{\infty} dwF(w) = -\frac{1}{2}F(0) - \frac{1}{12}F'(0) + \frac{1}{720}F'''(0) \quad (1.12)$$

From Appendix B, $F'(0) = 0$ and $F'''(0) = -4$, which gives

$$U(d) = -\frac{\pi^2\hbar c}{720d^3}L^2 \quad (1.13)$$

And the Casimir force is

$$F = -\frac{\partial U}{\partial d} = \frac{\pi^2\hbar c L^2}{240d^4} \quad (1.14)$$

This force was derived by using electromagnetic fluctuations [6].

CHAPTER TWO: REVIEW OF PRIOR CASIMIR FORCE INVESTIGATIONS

M.J Sparnaay. Attractive Forces between Flat Plates

The earliest attempt to measure the Casimir force was published in 1957 by Sparnaay [6], nine years after Casimir's paper. Parallel metal plates were used. The main difficulty in getting the plates close and pararallel was dust particles on the surfaces. Two aluminum parallel plates were used. One of them could be moved by using lever system. The other was attached to a spring system. The attractive force *K* was measured by using capacity methods, but the "surfaces asperities" prevented accurate measurement of the force.

If instead, two chromium or chromium-steel plates were used, the measurements indicated that Casimir's relation $K=Ad^{-4}$ was not contradicted. The constant *A* was found to have a value in the range 0.01 to 0.04×10^{-16}*dynes* cm^2, whereas the theoretical value is 0.013×10^{-10} *dynes* cm^2. The very large difference was attributed to the determination of the parallelism of the plates, whose separation was varied from 0.3 μm to 2 μm.

The materials of the two plates were chosen to be identical metals, because different metals would have different surfaces potentials and would attract each other according to $K_1=4.4\times10^{-5}P^2\ d^{-2}$, where *P* is the potential difference in millivolts and *d* is the separation in microns. The two plates were insulated so that the time constant (RC) of the discharge was much larger than one second. This required $R\gg 10^9$ Ohm [7].

Bressi et al. Measurement of the Casimir Force between Parallel Metallic Surfaces

Bressi et al. (2002) measured Casimir force between parallel metallic surfaces [8], Fig. 2. One of these was a cantilever beam (resonator) that was free to oscillate around its holding point. A second beam (source) was connected to a frame whose distance to the cantilever was controlled by a piezoelectric transducer (PZT). The silicon cantilever and the source were mounted within a vacuum chamber at a pressure of $\sim 10^{-5}$ mbar. The cantilever size was 1.9 cm x 1.2 mm x 47 μm with average roughness 10 nm. It was coated with a 50-nm-thick chromium layer and was fixed to a copper base. The source had the same "longitudinal" dimensions except for its thickness, which was 0.5 mm. It could be rotated by stepping motors around two axes to finely control the parallelism of the opposing surfaces. The source and the resonator were electrically connected to a voltage calibrator for the electrostatic calibrations. Alternatively, they were connected to an AC bridge for measuring the capacitance and for alignment by maximizing this capacitance at the minimum obtainable gap separation. The optical interferometer detected and quantified the motion of the cantilever [8].

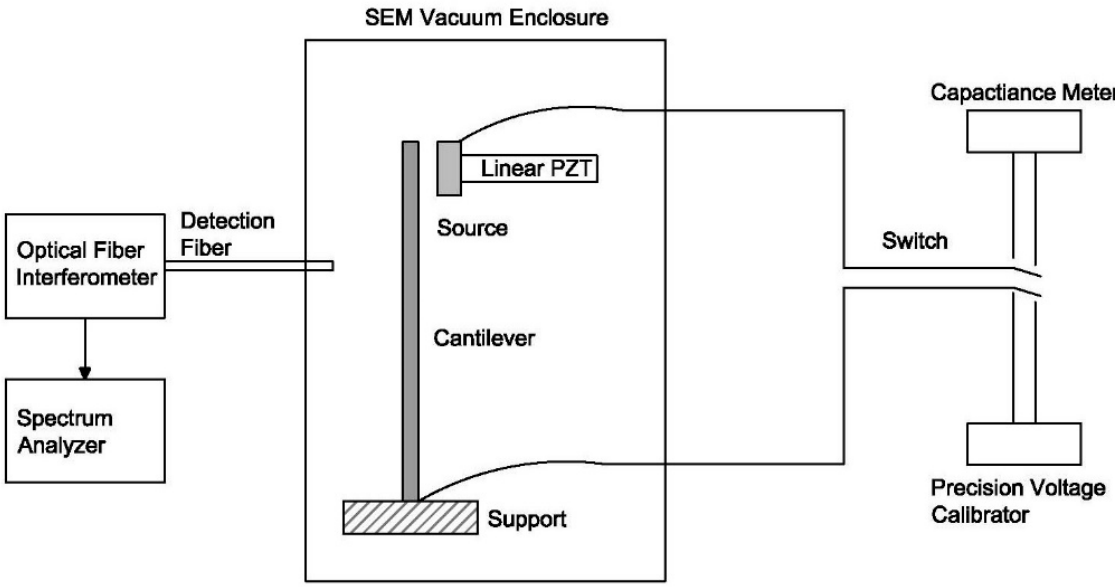

Figure 2: Experimental set up of Bressi et al [8].

The attractive Casimir force shifts the resonance frequency. The shift was measured as a function of separation over the range 0.5- 3.0 μm. The square of the shift is plotted as samples vs separation in Fig. 3. A residual electrostatic force contribution was zeroed by a dynamic technique. The result is shown in Fig.3 with the best fit with the function (2.1)

$$\Delta\nu^2(d) = -\frac{C_{cs}}{d^5} \tag{2.1}$$

The experimental verification of the Casimir prediction for the force between two parallel conducting surfaces in the 0.5 - 3.0 μm range leads to a measurement of the related coefficient with 15% precision.

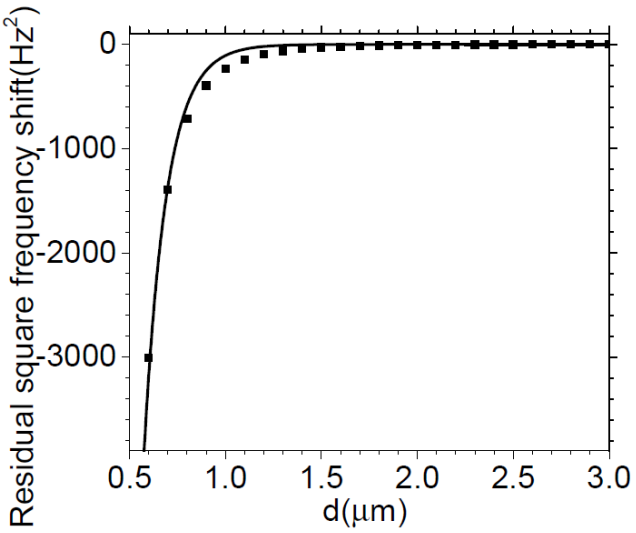

Figure 3: Square of the frequency shift as a function of separation for the experiment of Bressi et al [8].

U. Mohideen. Precision Measurement of the Casimir Force from 0.1 to 0.9 μm

Mohideen characterized the Casimir force using an atomic force microscope (AFM) [9]. The experiment consisted of a metallized sphere of diameter 196 μm and a flat plate. This arrangement has the advantage over parallel plates of not requiring alignment. The separation varied from 0.1 to 0.9 μm. The experiment was done at room temperature in vacuum at 50 mTorr pressure. The sphere was mounted on the tip of 300 μm long cantilever with Ag epoxy. A 1.25 cm diameter optically polished disk was used as the plate. The cantilever, the plate, and the sphere were coated with 300 nm of Al in an evaporator. Aluminum only was used on the cantilever because of its high optical

reflectivity throughout the visible spectrum. Surfaces of ball and plate were subsequently coated with < 20 nm layers of 60% Au and 40% Pd to prevent space charge effects due to patch oxidation of the Al coating. Deflection of the sphere and cantilever leads to a difference signal of the laser light density between photodiodes *A* and *B*. The sphere and plate were grounded to the AFM. The plate was moved towards the sphere in 3.6 nm steps and the difference signal recorded. The measured Casimir force is consistent within the uncertainty due to the finite conductivity and roughness of the metal surface. The procedure of measuring Casimir force was repeated for 26 scans in different locations of the flat plate [9].

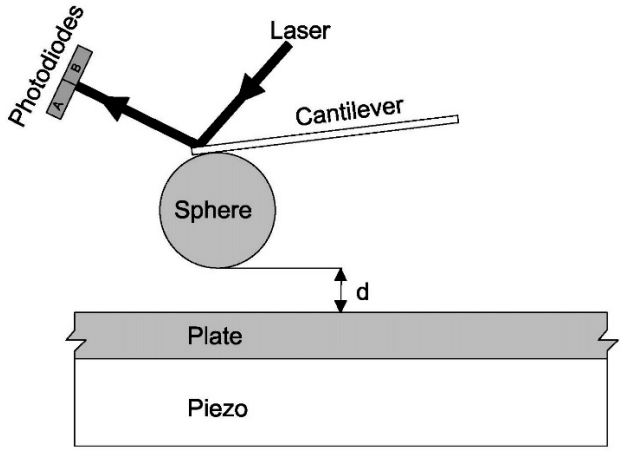

Figure 4: Schematic of metallized sphere mounted on an AFM cantilever above metal plate [9].

The average measured Casimir force as a function of sphere-plate separation from all the scans is shown in Fig. 5 as a solid squares. The theoretical Casimir force is shown as a solid line. The root mean square deviation $\sigma = \sqrt{(F_{exp} - F_{th})^2/N}$ is 1% at the

smallest surface separation can be taken as a statistical measure of the experimental precision where *N* is the number of data points.

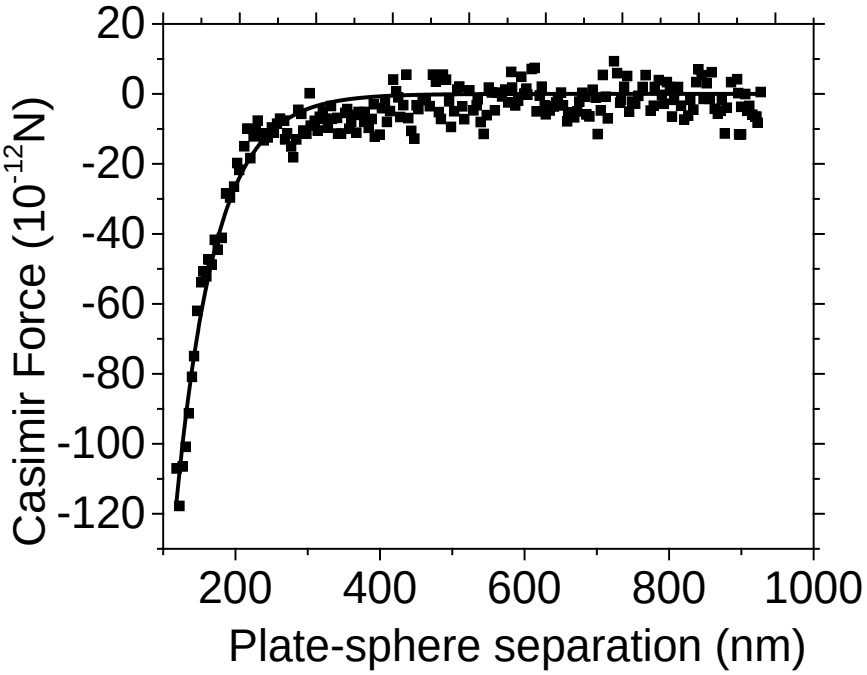

Figure 5: Force as a function of the distance moved by the plate. The solid line is the theoretical Casimir force. Experimental data are represented by square symbols [9].

J.Munday. Measured long-range repulsive Casimir–Lifshitz forces

Long-range *repulsive* Casimir force between a gold-coated sphere and a silica plate immersed in bromobenzene was measured. When the silica plate was replaced by a gold film, the force became attractive (Fig.6). The hydrodynamic force between the sphere and plate was used to calibrate the cantilever force constant and the surface separation at contact. A repulsive and attractive force in systems is satisfying the equation (2.2) [5].

$$-(\varepsilon_1 - \varepsilon_3)(\varepsilon_2 - \varepsilon_3) \quad (2.2)$$

.

Repulsive forces between macroscopic bodies can be qualitatively understood by considering their material polarizabilities or, their dielectric response functions: $\boldsymbol{\varepsilon}1$, $\boldsymbol{\varepsilon}2$ and $\boldsymbol{\varepsilon}3$according to Lifshitz's theory. The interaction of one of these bodies with the other across the third medium goes as a summation of terms with differences in material's permittivity Eq. (2.2) over frequencies ξ. Between two like materials, these terms are negative and correspond to attraction .However, when the dielectric response $\boldsymbol{\varepsilon}3$ of the medium is between $\boldsymbol{\varepsilon}1$ and $\boldsymbol{\varepsilon}2$

$$\varepsilon_{Au} > \varepsilon_{bromobenzene} > \varepsilon_{silica}$$

Then the $-(\varepsilon_1 - \varepsilon_3)(\varepsilon_2 - \varepsilon_3)$ terms are positive; the force is repulsive so that means the optical properties of gold, bromobenzene, and silica leads to a repulsive force between the gold and the silica surfaces, the limit for this repulsion is the case where region 2 ($\boldsymbol{\varepsilon}3$) is air or vacuum and the polarizability of medium 3 is less than that of substrate 1 [5].

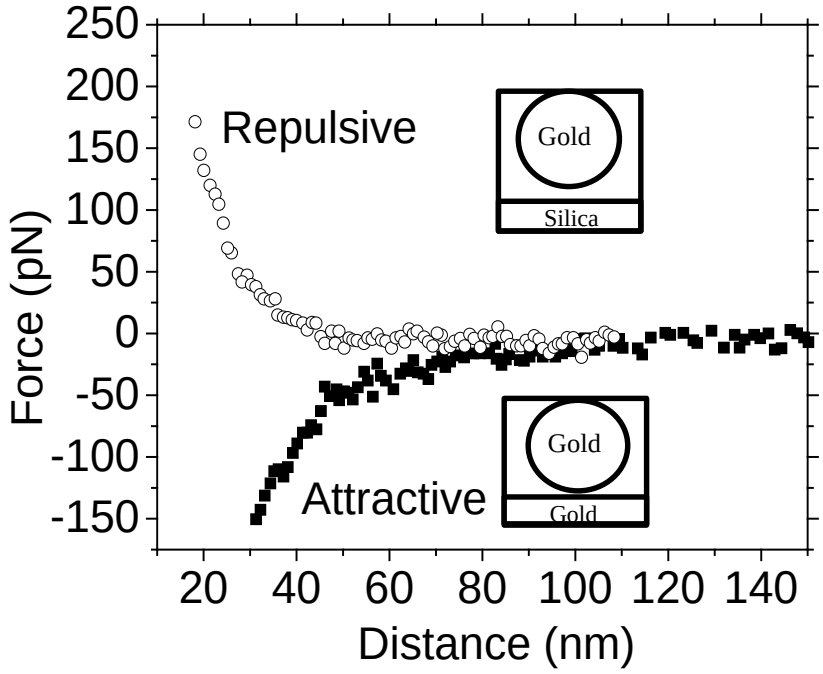

Figure 6: Measured repulsive (open circles) or attractive (solid square) Casimir force between a gold-coated (100 nm) polystyrene sphere and silica or gold-coated plate immersed in bromobenzene [5].

Ricardo. Measurement of the Casimir Force using a micromechanical torsional oscillator: Electrostatic Calibration

Decca and Lobez [10] have used electrostatic calibrations to perform Casimir interaction's measurements between a gold-plated sapphire sphere and a gold-coated polysilicon micromechanical torsional oscillator (Fig. 7). The electrostatic force between the surfaces is zeroed by applying a bias *V* between sphere and plate. Two independently contacted polysilicon electrodes are located under the oscillator plate to measure the capacitance between the electrodes and the plate. The springs are anchored to a silicon

nitride covered Si platform. The sphere is glued with conductive epoxy to the side of an Au-coated optical fiber, establishing an electrical connection between them. The entire setup is mounted into a can, where a pressure is less than 10^{-5} Torr.

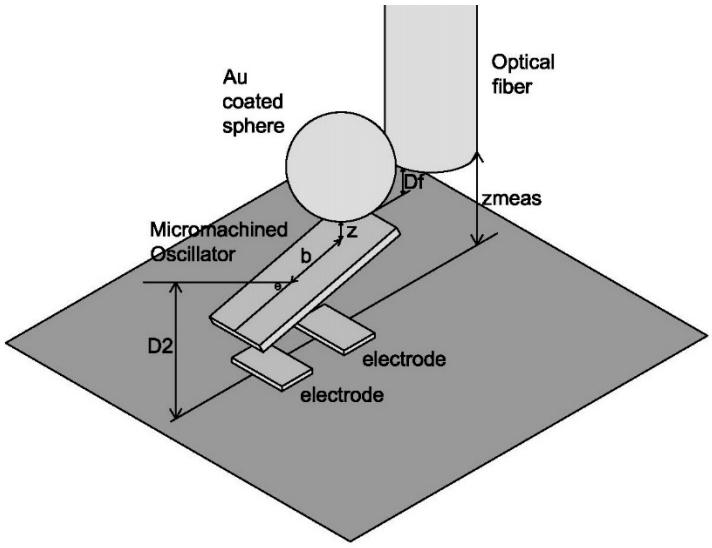

Figure 7: Schematic of experiment of Ref. [10].

The Casimir interaction between the Au-coated sphere and the Au-coated polysilicon plate can be performed by using the electrostatic calibrations. After performing the electrostatic calibrations the potential between the sphere and the plate is adjusted to be equal to the average residual potential so that electrostatic force is equal to zero within experimental error. After that the position of the sphere is changed by $\Delta z \sim 2$ nm, as measured by the interferometer. The actual z is calculated using the measured parameters by means of Eq. (2.3)

$$z = z_{means} - D1 - D2 - b\times\theta \qquad (2.3)$$

where D2 is measured interferometrically, b is measured optically and (θ) is measured by observing the changes in capacitance between the plate and the two underlying electrodes when the plate tilts under the influence of an external torque. At this value of *z* the Casimir interaction is obtained. The procedure is repeated for different values *z* until a curve of the interaction as a function of separation is built.

Different determinations of the Casimir interaction have been shown in figure 8. The force is measured by means of the deviation θ and the calibration of electrostatic force, while the pressure is determined by means of the change in the resonant frequency of the oscillator, and the calibration provided by the electrostatic interaction [10].

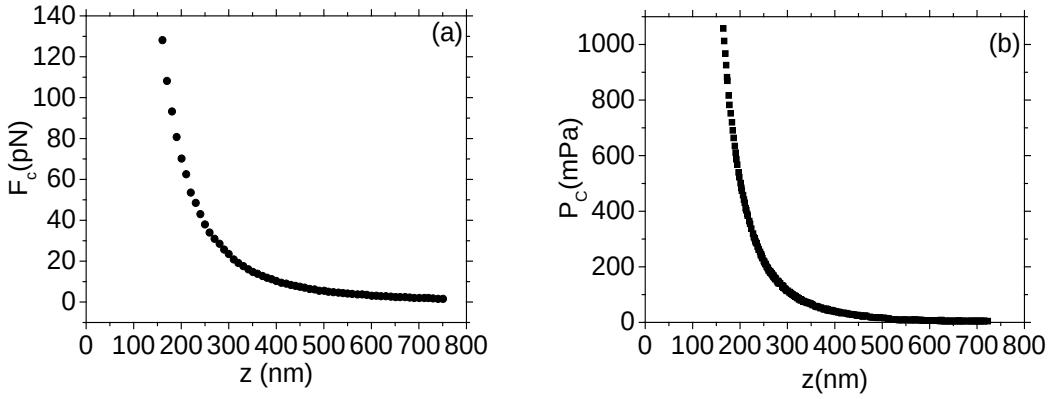

Figure 8: (a) Measured magnitude of $F_c(z)$ with respect to the separation of the sphere-plate configuration. (b) Determine magnitude of $P_c(z)$ between parallel plates using the sphere-plate configuration [10].

CHAPTER THREE: ESTIMATION OF CASIMIR FORCE FOR HypIR CANTILEVER

Figure 9 presents a scanning electron microscope (SEM) image of a MEMS cantilever device fabricated by our group at UCF. Shown is a single pixel of an infrared sensor described in [11, 12] and known as "HypIR". This particular example has characteristic lateral dimension 100 μm, and it was fabricated by photo-lithography.

Figure 10 presents an SEM image of a smaller pixel fabricated by electron beam lithography. This device has a paddle with lateral dimension 18 μm. The image clearly shows a tip at the central part of the paddle end. The tip is fabricated of gold and is attached to the underside of the paddle. In the image, this tip is in contact with a tip-pad on the surface, and it is the only part of the cantilever that contacts the surface besides the anchors at the ends of the folded arms. This is the intended resting unbiased state of the device, the so-called "null position".

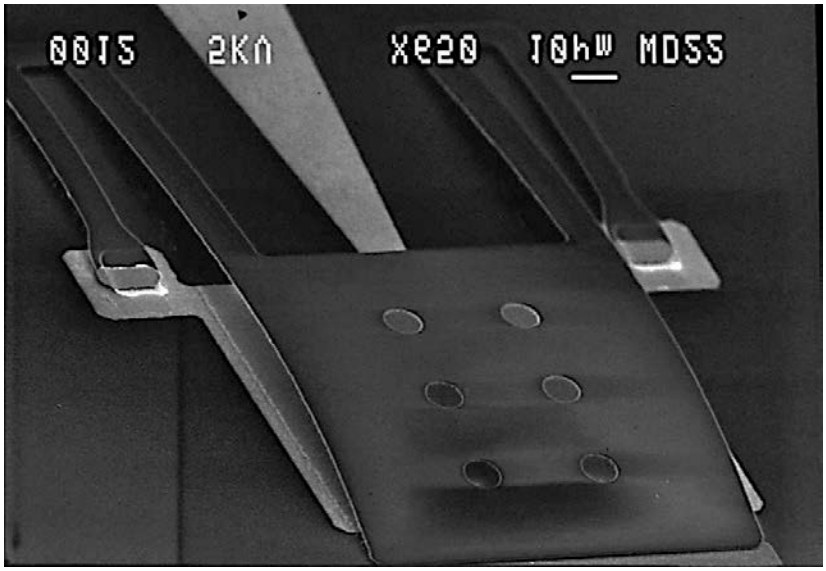

Figure 9: SEM image of MEMS cantilever with tip contact.

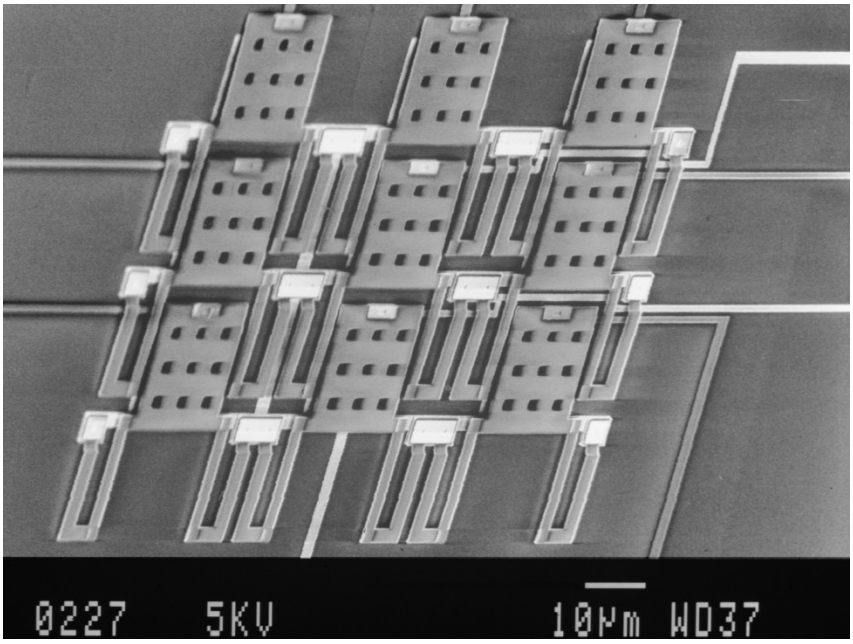

Figure 10: SEM image of MEMS cantilever with 18 μm x 18 μm paddle.

When an electric bias is applied, the tip is supposed to lift up from the surface by electrostatic repulsion. A more complete description of the elastic and electrostatic forces involved is presented in [11]. The Casimir force will cause there to be required an additional electric bias to release the tip from the surface. In other words, the Casimir force tends to make the surface more "sticky" than otherwise. A goal of this thesis is to estimate that effect. Our theoretical study is limited to the smaller of the two cantilevers (Fig. 10), for which the tip dimensions are 2 μm x 2 μm.

The separation z between the tip and the tip contact is supposed to be uniform and to be restricted to the range 2 nm < z < 2 μm. The lower separation limit is determined by the typical surface roughness of a commercial silicon wafer as determined by atomic force microscopy [12], and the larger separation limit is according to the intended

operational limit. The Casimir force is given by Eq. (1.14), in which L^2 is the area of the plates. Evaluating the constants, we find the force in Newtons to be

$$F = 5.2 \times 10^{-39} \ \text{N-m}^4/z^4. \tag{3.1}$$

The largest value of this force occurs at the 2 nm separation and has the value 0.325 mN (milliNewton). This is the force that must be overcome by electrostatic repulsion.

The Hyp-IR cantilever is supposed to be touching the surface in equilibrium. To lift the cantilever tip, the electrostatic force must also overcome the linear elastic restoring force F_E. For a force concentrated at one end of a beam, the spring constant K has the value $\frac{3EI}{L^3}$ [13], where E is Young's modulus, I is the area moment of inertia, and L is the length of the cantilever arms. For the arms, we ignore that they are folded, and we take the length to be L = 18 μm. The area moment of inertia $I = wt^3/12$, where w is the width and t is the thickness of the arms, so that $K = \frac{E.w.t^3}{4L^3}$. The width of the two arms together w = 4 μm, and their thickness t = 0.4 μm. Young's modulus for oxide E = 73 GPa. Thus, we find that K = 0.6 N/m.

The separation at which the elastic restoring force and the Casimir force are equal is found by setting Eq. (3.1) equal to Hooke's law. That distance is 24 nm. At this separation, both downward forces have the magnitude 14 nN. A log-log plot of these two forces is plotted as a function of z in Fig. 11. Their power law dependences with slopes of -4 and +1 are evident. Below 24 nm, the Casimir force is the dominant restoring force that opposes the electrostatic repulsive lifting of the tip.

Given the curvature of the cantilever evident in Fig. 9, and to some extent in Fig. 10, the entire tip is surely not parallel to the surface. Hence, the minimum 2 nm separation is probably not actually reached over most of the tip. Thus, the maximum estimated Casimir force is an upper bound for the Fig. 10 device. In fact, even the 24 nm distance of equal force is so small, that it is likely the elastic force dominates over the entire range of motion for a cantilever of the given shape and curvature.

Fig. 11 also presents the repulsive electrostatic force F_{ES} vs. tip height. This force is derived and discussed in the next section.

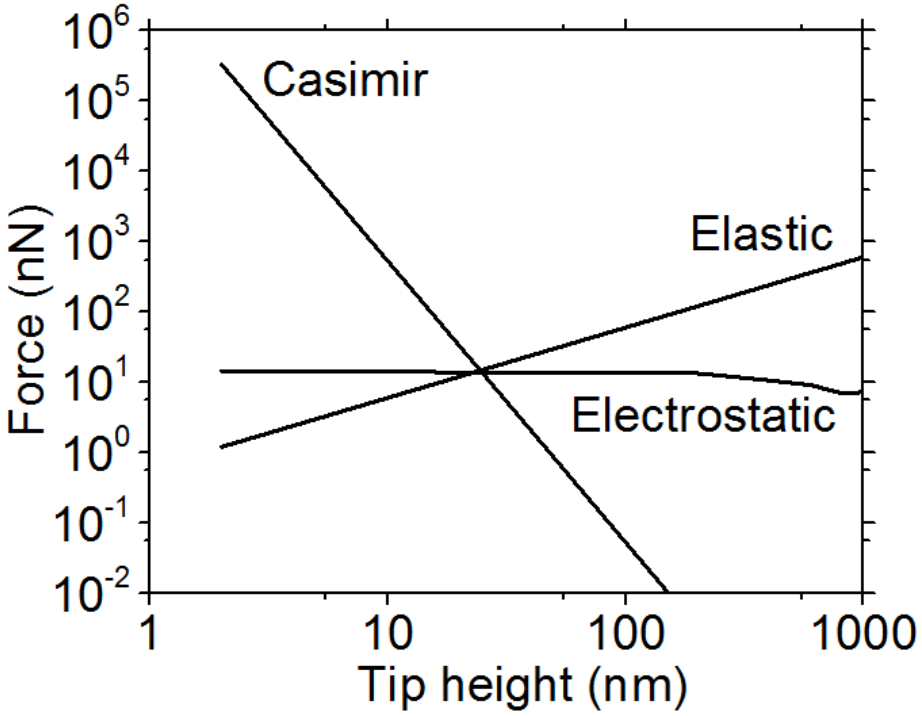

Figure 11: Log-Log plot comparing Casimir, Elastic, and Electrostatic forces with respect to tip height z.

Electrostatic force

Important to the intended function of the HypIR cantilever is that the upward repulsive electrostatic force be able to lift the tip against the attractive downward Casimir and elastic-restoring forces. A schematic model of the device is presented in Fig. 12. This model of the actual Fig. 10 device is comprised of three conductors: a fixed buried plate (1), a fixed surface plate (2), and a moveable cantilever (3). For simplicity, we assume all to have the same square shape and dimensions and that they are arranged parallel in a vertical stack with aligned edges. The surface plate and cantilever are biased at the same potential, and the buried plate is oppositely biased. The electrostatic repulsive force has been determined to be [14].

$$F_{ES} = \frac{V^2}{8}\left[\, 2\frac{\partial C_{23}}{\partial \zeta} + \frac{\partial C_{33}}{\partial \zeta} + \frac{\partial C_{22}}{\partial \zeta}\right] \tag{3.2}$$

Where ζ is the height of the cantilever metallization above the surface plate metallization, V is the applied bias voltage, C_{22} and C_{33} are the coefficients of capacity for the surface plate and moveable cantilever plate, respectively, and C_{23} is the coefficient of electrostatic induction between the surface plate and the cantilever. All three coefficients depend strongly on the position ζ of the cantilever metal. Contributions involving the other possible coefficients in the problem depend weakly on ζ and have been neglected.

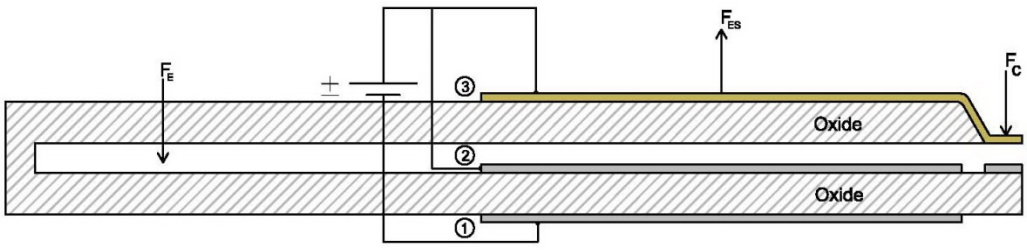

Figure 12: Schematic of model device for calculation purposes. The electrostatic portion of the device consists of three parallel plates with 18 μm x 18 μm dimensions. These are a fixed buried plate (1), a fixed surface plate (2), and a moveable cantilever (3). The separation of the surface plate and cantilever metal is ζ and has the minimum value 0.5 μm due to the structural oxide. The separation of the tip and tip contact is *z*.

Experimentally, we found the maximum allowed bias to be 40 V, beyond which dielectric breakdown destroys the device. We take the lateral dimensions of the electrostatic portion of the cantilever metals to be 18 μm x 18 μm. The thickness of the metal on the fabricated cantilever is 100 nm, and it sits on 0.5 μm of structural oxide, so that $\zeta = z + 0.5$ μm. We ignore the effect of oxide permittivity for now.

The coefficients in Eq. (3.2) are calculated numerically as a function of ζ using the finite element method (FEM) software Elmer [15]. These data are plotted in Fig. 13(left), where the neglected coefficients are also plotted to confirm their weak ζ dependence. Fig. 13 (inset) shows a log-log plot of the three most important coefficients in Eq. (3.2). Note that the slope of C_{23} is positive and its magnitude exceeds the magnitudes of the negative slopes for C_{22} and C_{33}. Hence, Eq. (3.2) is positive and the electrostatic force is repulsive.

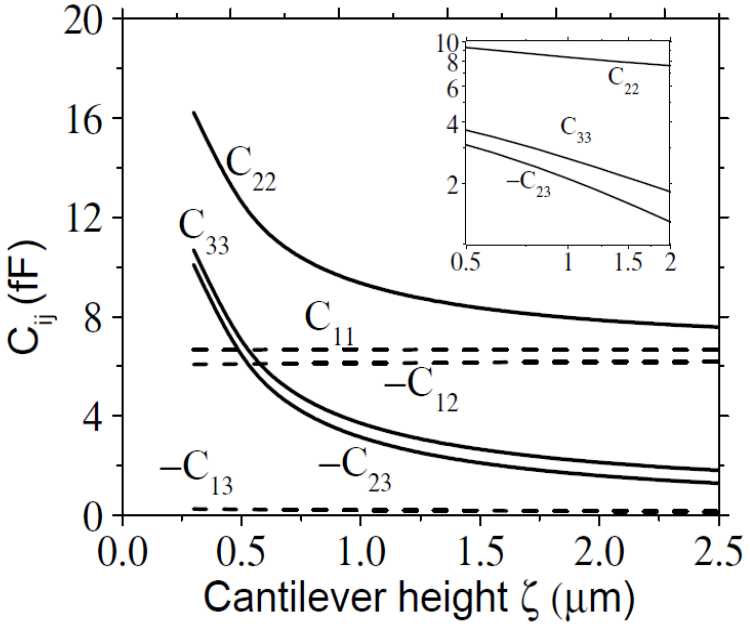

Figure 13: The capacitance and electrostatic induction coefficients with respect to the separation ζ. The inset presents a log-log plot for three of the coefficients.

The electrostatic force calculated from Eq. (3.2) for V = 40 V is plotted Fig. 14 for the cantilever metal height range 0.5 μm < ζ < 2.5 μm. This range corresponds to the range of tip-heights ~0 < z < 2.0 μm. The curve is an exponential fit to the calculation data, which have unphysical periodic variations due to numerical artifacts. This curve is plotted also in Fig. 11.

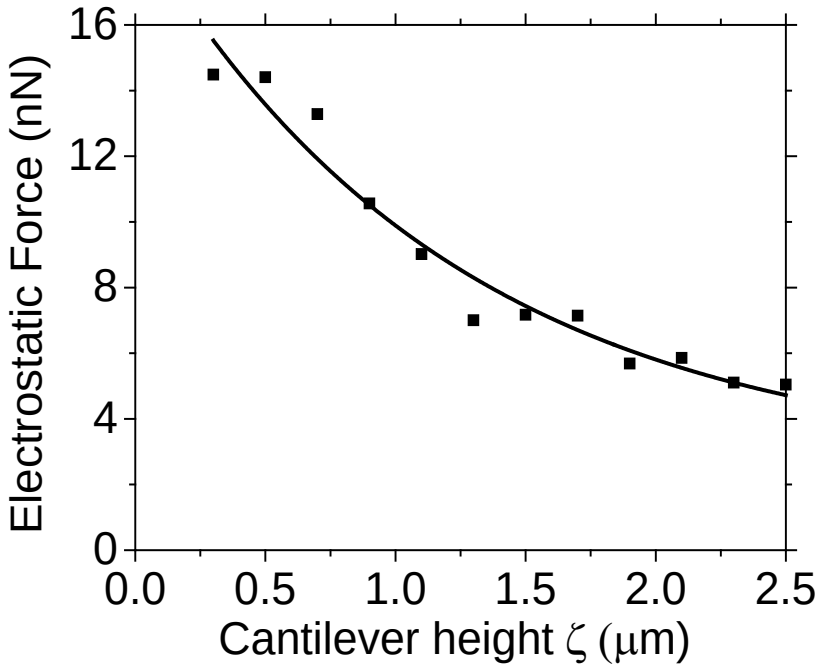

Figure 14: Electrostatic force vs. ζ for the maximum permissible applied bias of 40 V.

According to Fig. 11, the repulsive electrostatic force is smaller than the Casimir force below a tip height of z = 24 nm. Accordingly, the tip should not ever lift based assuming the model design. That the cantilevers of Figs. 9 and 10 have been observed by video microscopy and electric response [14] to lift from the surface is because they are non-ideal. Residues and curvature cause the effective minimum separation of tip and tip-pad to significantly exceed 24 nm.

According to Fig. 11, the electrostatic force is smaller than the elastic restoring force for values of z > 24 nm. For this reason, too, electrostatic repulsion should fail to lift the cantilever. That the cantilever does lift indicates that the actual cantilever is

longer and floppier than the model, which is not surprising considering that their folded structure was ignored. Secondly, the electrostatic force is actually distributed over the cantilever plate (which is itself flexible) and not concentrated at the end of the arms as assumed. Thirdly, we have ignored the role of the oxide, which will be shown in the next chapter to give stronger repulsive force.

CHAPTER FOUR: FORCE OPTIMIZATION

This chapter considers more realistic calculations, which include the 0.5 μm oxide layers between buried- and surface-plates and on the underside of the cantilever. The minimum air gap was taken to be zero. The coefficients of capacity and electrostatic induction are plotted in Fig. 15 as a function of ζ. In comparison with Fig. 13, the magnitudes of all the coefficients of the capacitance are increased by the presence of the oxide layers.

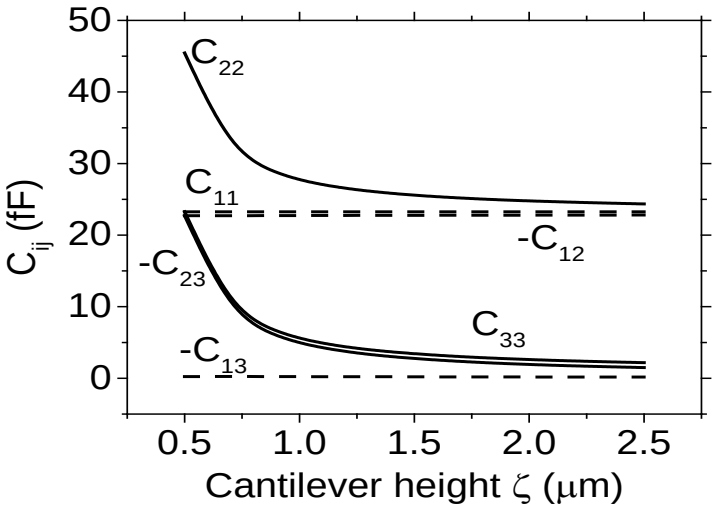

Figure 15: the capacitance and the electrostatic inductions vs. the gap ζ.

The three coefficients of most importance to the force in Eq. (3.2) are plotted in Fig. 16 and compared with those lacking oxide. The effect of oxide is most noticeable at small ζ. At large ζ, the curves for C_{33} with and without oxide, and similarly for C_{23}, approach each other.

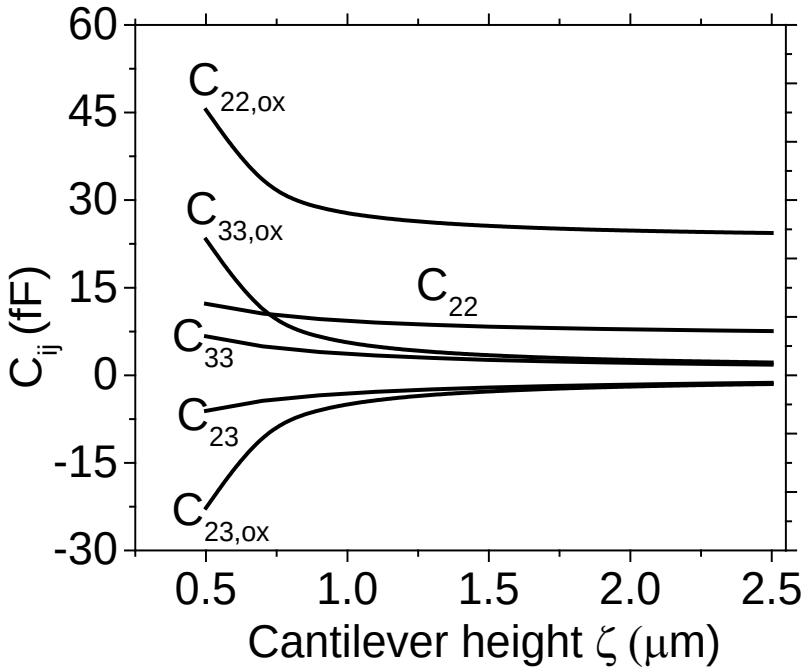

Figure 16: Coefficients of capacitance and of electrostatic induction with strong dependence on cantilever displacement. The three terms with (without) subscript "ox" are the results of calculations for devices with (without) oxide.

Fig. 17 presents the electrostatic force calculated from Eq. (3.2) and compares it to the results without oxide. Electrostatic force is higher with oxide, especially at small ζ. The difference is a factor of 3.9 at $\zeta = 0.5$ μm.

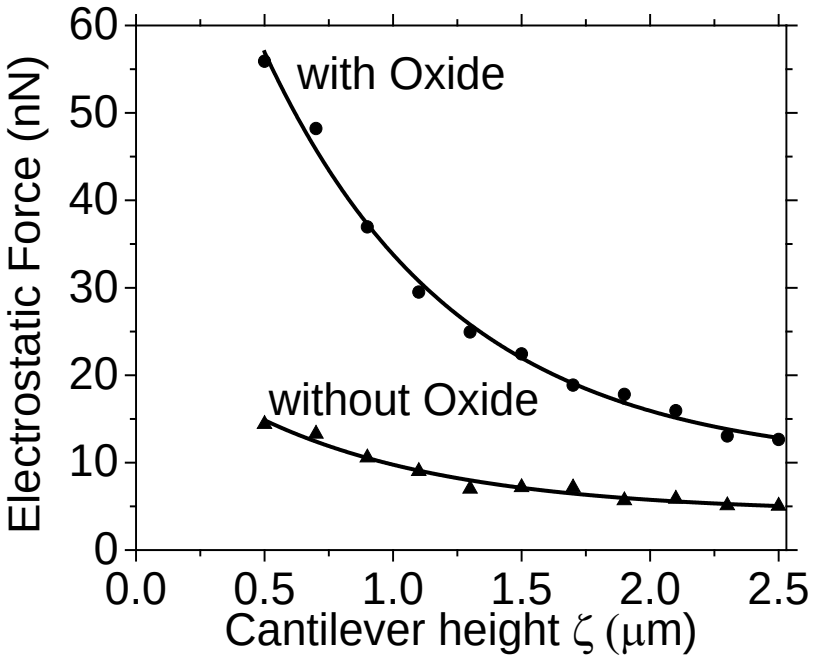

Figure 17: Electrostatic repulsive force vs. ζ with and without the structural oxide.

Fig. 18 presents a plot of the three forces, where the electrostatic force calculation included the structural oxide, as a function of tip height z. In comparison to Fig. 11, we now find a finite range 18 nm < z < 100 nm over which the repulsive electrostatic force exceeds the other two attractive forces. To lift the tip beyond 0.1 μm, as desired for HypIR device function, the cantilever should be made less stiff. To insure the tip can be lifted from the surface, the roughness of the tip pad should exceed 18 nm. Alternatively, the tip area can be made smaller, as considered next.

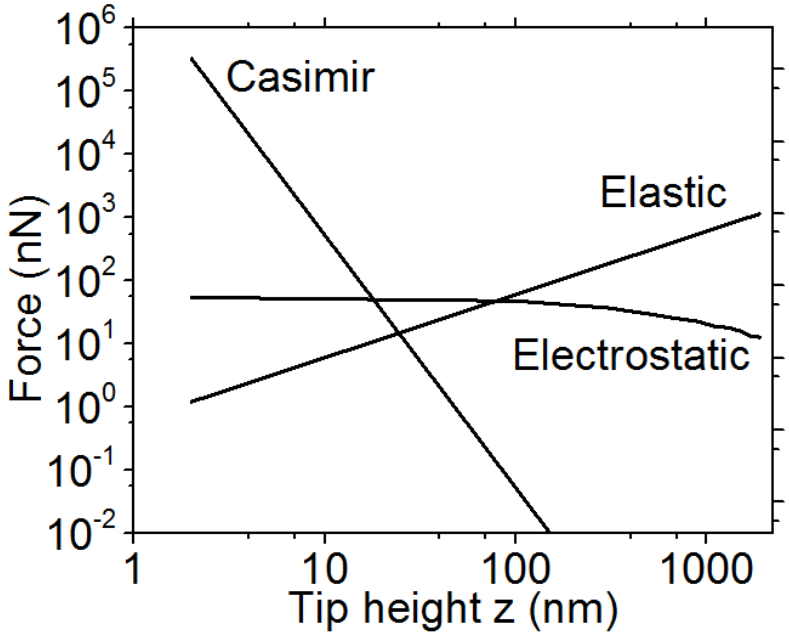

Figure 18: Log-Log plot comparing Casimir, Elastic, and Electrostatic forces, with oxide included, as a function of tip height *z*, for tip area 2 μm x 2 μm.

If we assume a sharp tip with dimensions 25 nm x 25 nm, then at z = 2 nm the Casimir force will be 50 nN as in Fig. 19. This is now less than the electrostatic force, so that the cantilever should easily lift. The maximum height is still 100 nm, so that we still need arms that are less stiff.

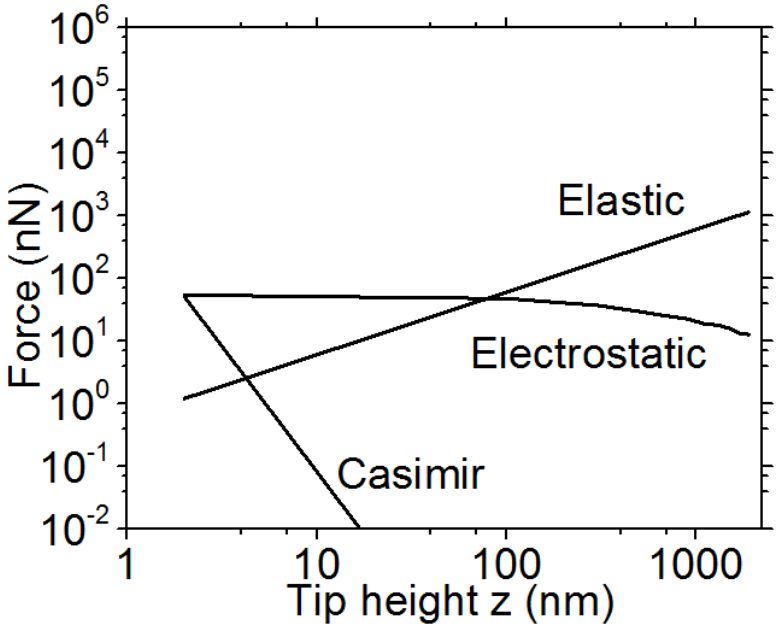

Figure 19: Log-Log plot of Casimir, Elastic, and Electrostatic forces vs. the tip height *z* for tip area 25 nm x 25 nm.

CHAPTER FIVE: SUMMARY

The Casimir force causes attraction between two metal surfaces at very short distances of separation. It is considered to be a "contact" force. It is a quantum electrodynamics phenomenon that arises from zero-point energy of the harmonic oscillators that are the normal modes of the electromagnetic field. Such "contact" force creates difficulties in the operation of certain MEMS and NEMS (micro and nano electromechanical systems) because attractive Casimir force leads to stiction (adhesion) between the surfaces of MEMS and NEMS devices.

This thesis presented a derivation for the formula for the Casimir force, which depends strongly on contact area and on separation of the two surfaces. This thesis also reviews many of the papers that presented studies of the Casimir force studies for different geometries by experiment and numerical methods. The new science in this thesis is the evaluation of the Casimir attractive force for single pixel of an infrared sensor known as "HypIR" that was fabricated by our group at UCF.

HypIR is a MEMS cantilever with a metallic tip that contacts a metallic tip pad. When an electric bias is applied, the tip is supposed to lift up from the surface by electrostatic repulsion, but to do so requires that it overcome both the Casimir sticking force and the elastic restoring force. The three forces were compared theoretically for geometry as close as practical to that of the actual cantilever that was fabricated. Calculations were performed with and without considering the permittivity of the structural oxide, and it was found that the oxide significantly increases the repulsion. Nevertheless, the results suggest that the cantilever tip should remain stuck to the surface

for any electrostatic force available for the allowed range of applied bias, unless the tip area can be made as small as 25 nm x 25 nm. That the cantilever is observed to lift under applied bias is a consequence of imperfections in the fabrication that cause the contact area to be much smaller than anticipated and/or the separation at contact to be significantly more than the assumed minimum of 2 nm.

APPENDIX A: EIGEN FREQUENCIES OF A CUBOIDAL RESONATOR WITH PERFICTLY CONDUCTING WALLS

This derivation follows [16]. The electric field inside the cavity satisfies the wave equation

$$\nabla^2 E + \frac{1}{c^2}\frac{\partial^2 E}{\partial t^2} = 0 \qquad \text{(A1)}$$

And

$$\mathbf{Div\ E} = 0 \qquad \text{(A2)}$$

(Since there is no charge in the cavity). The boundary conditions for perfectly conducting walls are

$$\mathbf{E}_t = 0, \quad H_n = 0 \qquad \text{(A3)}$$

The solution that satisfies (A1-3) is

$$E_x = A_1 \cos k_x x \sin k_y y \sin k_z z\, e^{-i\omega t} \qquad \text{(A4)}$$

The other components found from cyclic permutation of x,y,z and the magnetic field found from

$$\mathbf{H} = -i\,(c/\omega)\ \mathbf{curl\ E} \qquad \text{(A5)}$$

The wave vectors are $k_x = n_1\,\pi/a_1$, where a_1 is the length of the box in the x-direction. The other two components are similarly defined. The frequency of the wave is

$$\omega^2 = c^2\,(k_x^2 + k_y^2 + k_z^2) \qquad \text{(A6)}$$

Equation (A2) gives the condition

$$A_1 k_x + A_2 k_y + A_3 k_z = 0, \qquad (A7)$$

so that only two of the undetermined coefficients A_1, A_2, A_3 are independent.

If none of the n_1, n_2, n_3 are zero, and the coefficients A_1, A_2 are chosen and fixed, with A_3 determined by Eq. (A7), then there is another set of coefficients $A_1' = A_2\, k_y/k_x$ and $A_2' = A_1\, k_x/k_y$ with the same A_3 that also satisfies Eq. (A7) with the same frequency. Thus, each frequency is doubly degenerate in this case.

If one of the n_1, n_2, n_3 is zero, then only one of the components of $\mathbf{E}$ is non-zero. Then there is only one undetermined coefficient, and once this is chosen and fixed, there are no other modes with the same frequency. Such modes are non-degenerate.

If two of the n_1, n_2, n_3 are zero, then at least one of the sine terms in each component of $\mathbf{E}$ will be zero, so that $\mathbf{E} = 0$. This means that there are no modes propagating along any of the cube axes. The lowest frequency is one where one of the n_1, n_2, n_3 is zero and the other two are 1

APPENDIX B: EULER -MACLAURIN FORMULA

The Euler-Maclaurin formula [17]

$$\sum_{k=1}^{n} t(k) - \int t dn = \frac{1}{2}t + \frac{1}{12}\frac{dt}{dn} - \frac{1}{720}\frac{d^2t}{dn^2} + \cdots \quad \text{(B1)}$$

Where n is natural number and $t(k)$is analytic function for $k > 0$, gives a relation between the integral and the sum of a function. It is applied to provide the approximate integral by finite sums or to evaluate infinite series by using integrals. To derive it, define

$$S(n) \equiv \sum_{k=1}^{n} t(k) \quad \text{(B2)}$$

And expand $S(x)$ as Taylor series about point n, then evaluate it at x = n - 1 to get:

$$S(n-1) = S(n) - S'(n) + \frac{1}{2!}S''(n) - \frac{1}{3!}S'''(n) + \cdots \quad \text{(B3)}$$

Then

$$\boldsymbol{t(n) = S(n) - S(n-1) = \frac{dS}{dn} - \frac{1}{2!}\frac{d^2S}{dn^2} + \frac{1}{3!}\frac{d^3S}{dn^3} + \frac{1}{4!}\frac{d^4S}{dn^4} + \cdots} \quad \text{(B4)}$$

According to Euler, $\boldsymbol{S}$ can be expressed as [14]

$$\boldsymbol{S = \int t dn + \alpha t + \beta\frac{dt}{dn} + \gamma\frac{d^2t}{dn^2} + \delta\frac{d^3t}{dn^3}} \ \ldots$$

where $\boldsymbol{\alpha, \beta, \gamma,}$ **and** $\boldsymbol{\delta}$ are real number coefficients.

By applying eq. (2) in eq. (1) and using undetermined coefficient method (this method is used to find the particular solution coefficient for the differential equations to find $\alpha, \beta, \gamma, \delta$ we get

$$t = \left(t + \alpha\frac{dt}{dn} + \beta\frac{d^2t}{dn^2} + \gamma\frac{d^3t}{dn^3} + \delta\frac{d^4t}{dn^4}\right) - \frac{1}{2!}\left(\frac{dt}{dn} + \alpha\frac{d^2t}{dn^2} + \beta\frac{d^3t}{dn^3} + \gamma\frac{d^4t}{dn^4} + \delta\frac{d^5t}{dn^5}\right) + \frac{1}{3!}\left(\frac{d^2t}{dn^2} + \alpha\frac{d^3t}{dn^3} + \beta\frac{d^4t}{dn^4} + \gamma\frac{d^5t}{dn^5} + \delta\frac{d^6t}{dn^6}\right) - \frac{1}{4!}\left(\frac{d^3t}{dn^3} + \alpha\frac{d^4t}{dn^4} + \beta\frac{d^5t}{dn^5} + \gamma\frac{d^6t}{dn^6} + \delta\frac{d^7t}{dn^7}\right) + \frac{1}{5!}\left(\frac{d^4t}{dn^4} + \alpha\frac{d^5t}{dn^5} + \beta\frac{d^6t}{dn^6} + \gamma\frac{d^7t}{dn^7} + \delta\frac{d^8t}{dn^8}\right)$$

So

$$t = t + \frac{dt}{dn}\left(\alpha - \frac{1}{2!}\right) + \frac{d^2t}{dn^2}\left(\beta - \frac{1}{2!}\alpha + \frac{1}{3!}\right) + \frac{d^3t}{dn^3}\left(\gamma - \frac{1}{2!}\beta + \frac{1}{3!}\alpha - \frac{1}{4!}\right) + \frac{d^4t}{dn^4}\left(\delta - \frac{1}{2!}\gamma + \frac{1}{3!}\beta - \frac{1}{4!}\alpha + \frac{1}{5!}\right)$$

Now we can get

$$\alpha - \frac{1}{2!} = 0 \Rightarrow \alpha = \frac{1}{2}$$

$\beta - \frac{1}{2!}\alpha + \frac{1}{3!} = 0 \Rightarrow \beta = \frac{1}{12}$ (By using the value ofα)

$\gamma - \frac{1}{2!}\beta + \frac{1}{3!}\alpha - \frac{1}{4!} = 0 \Rightarrow \gamma = 0$ (By using the value of$\alpha\ and\ \beta$)

$$\delta - \frac{1}{2!}\gamma + \frac{1}{3!}\beta - \frac{1}{4!}\alpha + \frac{1}{5!} = 0 \Rightarrow \delta = -\frac{1}{720}$$

Finally, Euler –Maclaurin formula could be written as

$$S = \int t dn + \frac{1}{2}t + \frac{1}{12}\frac{dt}{dn} - \frac{1}{720}\frac{d^3t}{dn^3} + \cdots$$

LIST OF REFRENCES

[1] P.W. Milonni and M. Shih, "'Casimir forces," *Contemporary Physics*, vol. 33, no. 5, pp. 313-322.

[2] S.K. Lamoreaux, "'Demonstration of the Casimir Force in the 0. 6 to 6 μm Range," *Phys.Rev.Lett.*, vol. 78, no. 1, pp. 5-8.

[3] M.J. Madou, "'Fundamentals of microfabrication: the science of miniaturization,", 2002.

[4] L.D. Landau and E.M. Lifshi͡ts, "'The classical theory of fields,", vol. 2, Elsevier, 1975.

[5] J.N. Munday, F. Capasso and V.A. Parsegian, "'Measured long-range repulsive Casimir–Lifshitz forces," *Nature*, vol. 457, no. 7226, pp. 170-173.

[6] E. Lifshitz and L. Pitaevskii, "'Statistical Physics part 2, Landau and Lifshitz course of Theoretical physics,".

[7] M. Sparnaay, "'Attractive forces between flat plates,". Nature, 180, 334-335, 1957.

[8] G. Bressi, G. Carugno, R. Onofrio and G. Ruoso, "'Measurement of the Casimir force between parallel metallic surfaces," *Phys.Rev.Lett.*, vol. 88, no. 4, pp. 041804.

[9] U. Mohideen and A. Roy, "'Precision measurement of the Casimir force from 0.1 to 0.9 μ m," *Phys.Rev.Lett.*, vol. 81, no. 21, pp. 4549.

[10] R.S. Decca and D. LOPez, "'Measurement of the Casimir force using a micromechanical torsional oscillator: electrostatic calibration," *International Journal of Modern Physics A*, vol. 24, no. 08n09, pp. 1748-1756.

[11] E. Smith, J. Boroumand, I. Rezadad, P. Figueiredo, J. Nath, D. Panjwani, R. Peale and O. Edwards, "'MEMS clocking-cantilever thermal detector,", pp. 87043B-87043B-4.

[12] R. Peale, O. Lopatiuk, J. Cleary, S. Santos, J. Henderson, D. Clark, L. Chernyak, T. Winningham, E. Del Barco and H. Heinrich, "'Propagation and out-coupling of electron-beam excited surface plasmons on gold,".

[13] M. Gedeon, "'Cantilever Beams Part 1 - Beam Stiffnes, no. 20.

[14] I. Rezadad, J. Boroumand, E. Smith, A. Alhasan and R. Peale, "'Repulsive electrostatic froces in MEMS cantilever IR sensors,", vol. 9070, no. 57.

[15] "http://www.csc.fi/english/pages/elmer/index_html,".

[16] E. Lifshitz, L. Pitaevskii and L. Landau, "Electrodynamics of Continuous Media: Volume 8," Elsevier, 2008.

[17] R. Roy, "'Sources in the Development of Mathematics,". New York: Cambridge University Press, 2011. Print.